Three-body recombination of spin-polarized atomic hydrogen in very strong magnetic fields

J. D. Gillaspy and Isaac F. Silvera

Lyman Laboratory of Physics, Harvard University, Cambridge, Massachusetts 02138

J. S. Brooks

Physics Department, Boston University, Boston, Massachusetts 02215
(Received 24 October 1988)

The study of spin-polarized atomic hydrogen in the three-dimensional gas phase has been extended into a new regime of magnetic field strength. Analysis of decay data for $B = 10$–20 T reveal for the first time the characteristic peak in the three-body dipolar-decay rate constant as predicted by Kagan, Vartanyants, and Shlyapnikov (Zh. Eksp. Teor. Fiz. **81**, 1113 (1981) [Sov. Phys.—JETP **54**, 590 (1981)]). Beyond 17 T we observe a rapid falloff of the three-body-decay rate constant. We also determine a value for the three-body-exchange rate constant which is in accord with the calculation of Kagan *et al*. In contrast to the picture which was emerging from previous studies at more moderate fields, the data presented here suggest that existing theories are capable of describing the decay of the system in the very-high-field limit. The new picture which is emerging suggests that Bose-Einstein condensation may be achievable at somewhat higher fields which are currently available at high-magnetic-field facilities.

I. INTRODUCTION

The past several years have been witness to several intense experimental efforts to observe Bose-Einstein condensation (BEC) in spin-polarized atomic hydrogen ($H\downarrow$).[1-4] Predicted over six decades ago in Einstein's classic paper,[5] BEC has never been observed in a dilute atomic system such as $H\downarrow$. The spectacular quantum properties of superfluid helium have been interpreted in terms of BEC; however, because of the strong interactions in this high-density system, the ground state is complex and analysis of its properties is formidable and challenging. In contrast, the properties of the weakly interacting Bose gas are easily analyzed.[6] The achievement of BEC in $H\downarrow$ would certainly provide the scientific community with an exciting new quantum system in which to test some fundamental ideas of modern physics.

The critical condition necessary for BEC at a given gas density (n) is that the thermal de Broglie wavelength, $\lambda = (2\pi\hbar^2/mkT)^{1/2}$, be made large enough to span the average interparticle spacing (or more precisely, $n\lambda^3 = 2.16$). Since the first experiments of Silvera and Walraven,[7] $H\downarrow$ densities have been increased by over 4 orders of magnitude, but still lie at least a factor of 35 short of those needed for BEC.[4] The experimental efforts have been thwarted by the presence of rapid three-body recombination into the molecular state. Recombination depletes the atoms from the gas phase and liberates excessive internal energy which overheats the samples and eventually leads to small-scale explosions of the gas.[1,4] At high densities, three-body recombination occurs primarily in the bulk phase of the gas, whereas at low-temperatures surface recombination dominates.

Recent efforts to remove the surface decay problem by confining the hydrogen gas in a magnetic trap have been reported by Hess *et al.*,[8] Masuhara *et al.*,[9] and van Roijen *et al.*[10] In order to observe BEC in these intrinsically low-density traps, robust cooling techniques must be developed to lower the temperature of the gas by several orders of magnitude. In the work discussed in this paper, we focus on the more moderate-temperature (high-density) approach to BEC. No attempt has been made to achieve BEC in this work, as we have concentrated our efforts on understanding the limiting recombination processes.

In previous high-density experiments of Sprik *et al.*,[1] Hess *et al.*,[3] Bell *et al.*,[3] and Tommila *et al.*,[4] the main three-body recombination process was believed to be mediated by the dipole-dipole interaction which has been calculated by Kagan *et al.*,[11] de Goey *et al.*,[12,13] and Stoof *et al.*[14,15] The main contribution to the dipolar-recombination rate constant at the magnetic field strengths used in the experiments mentioned above is believed to be one in which ortho-H_2 molecules are formed in a state with vibrational quantum number $v = 14$ and rotational quantum number $J = 3$.[11] In a collision either one or two atoms can have their electron spins flipped. The dominant two-spin-flip process should be cut off (to zero) in magnetic fields of 25–27 T whereas the one-spin-flip process is cut off at fields twice as high. The cutoff is forced by the conservation of energy and is very insensitive to the details of the calculations: When the Zeeman spin-flip energy exceeds the depth of the final bound-state energy level, then that decay channel simply becomes inaccessible at low temperatures. The theories predict that the cutoff should be preceded by a peak at fields near 15 T (the experiments mentioned above have extended up to about 10 T). In an earlier work,[16] we have shown that if the theories are correct, BEC might be achieved with the application of currently available fields

(25–27 T) if the proper experimental strategy is followed. The present article details our experimental effort at the Francis Bitter National Magnet Laboratory (FBNML) to explore the possibilities which may exist for observing BEC in very strong magnetic fields.[17]

In this paper we show that for fields above 10 T there is reasonably good agreement between theory and experiment. The field dependence given by the theoretical calculations mentioned above are in poor agreement with experiments at moderate field strengths (up to 10 T). The experiments show a rate constant decreasing rather than increasing, with increasing field. Recent theoretical work has suggested that the neglect of collisional rearrangement processes in the calculations at moderate field strengths might account for the discrepancy.[14] If so, then a more exact calculation could yield significantly different results at moderate fields, while preserving the cutoff behavior at high fields. The theoretical work of de Goey et al.[18] is a step in this direction, and seems to qualitatively confirm these ideas.

II. EXPERIMENTAL APPARATUS

A. Overview

Our technique consists of compressing a volume of atomic hydrogen gas into a small bubble which is held submerged under the surface of a pool of superfluid ^{4}He at low temperature and high-magnetic field. As the atoms recombine to form molecules, they exit the bubble through the surface and the bubble shrinks in volume. We monitor the volume and analyze the resulting decay curve to extract information about the decay processes. Similar techniques have been used earlier.[1,4]

B. The magnets

Very large static magnetic fields are required for this experiment. The magnets we use are of the Bitter-plate design[19] measuring 2 ft in external diameter, and possessing a 2-in. inner-diameter room-temperature access bore. The peak field we achieve in such a magnet is 20 T. Higher fields (up to $\sim$30 T) have been achieved by nesting a Bitter magnet in a large superconducting magnet to provide an additional background field; however, we have not used such a hybrid magnet system in this work. We have made extensive use of an 8-T superconducting magnet to test the performance of our apparatus prior to use in the Bitter magnets.

A single Bitter magnet can be powered by four 10-kA generators connected in parallel to yield at total continuous power of 10 MW. The power is fed to the magnet by eight water-cooled cables which measure about three inches in diameter. The magnet itself is cooled by an internal flow of several thousand gal/min of purified water provided by eight fire hoses; this flow leads to significant vibration in the magnetic housing and great care had to be taken to avoid coupling of these vibrations to the refrigerator and the measuring devices in the experiment.

Although the dc current through the magnets is stable

to 0.1%, the large magnitude of the field and the presence of unwanted ac components up to 720 Hz can give rise to field derivatives as high as 2 T/sec. Such large-field derivatives can generate significant eddy-current heating in metals, and present a formidable cryogenic problem. Our means of overcoming this problem is discussed in Sec. II D below.

The series of measurements described in this paper consumed the largest yearly portion of run time over allowed a single user of the FBNML, yet by the usual standards of spin-polarized hydrogen research, our data collection time was exceedingly short, resulting in larger standard deviations of the experimental results.

C. The refrigerator

We use a conventional dilution refrigerator (S.H.E. Corporation) of modest cooling power (100 μW at 100 mK) which has been modified for use with the Bitter magnet (Fig. 1). The narrow tail piece which extends into the Bitter magnet is shown in a cross-sectional top view at the position of the cell in the field center in Fig. 2. Since all of the experiments discussed here were performed above 0.5 K, we run the refrigerator without a

Legend:

⬛⬛⬛⬛ = Atomic Hydrogen Discharge

⊠ ⊠ = Magnet

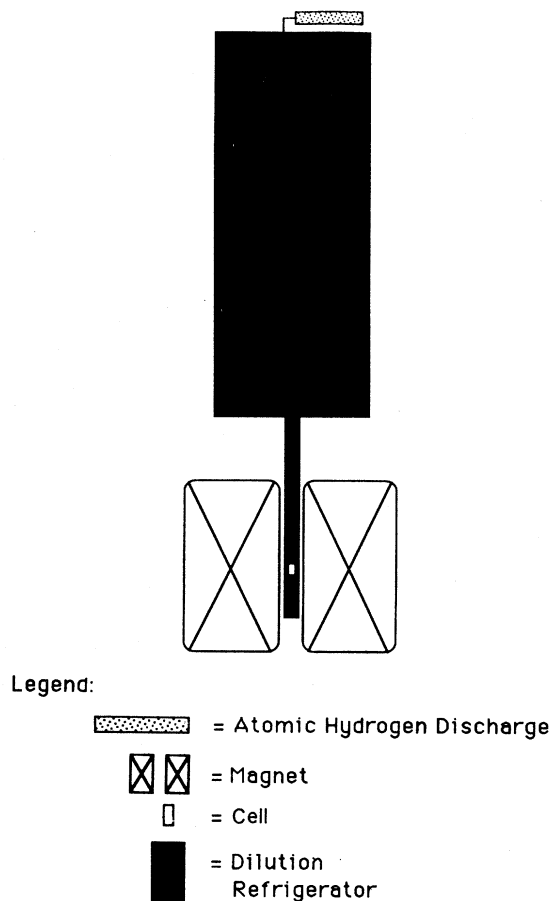⬚ = Cell

⬛ = Dilution Refrigerator

FIG. 1. Cross-sectional view of dilution refrigerator with atomic hydrogen experiment in a Bitter magnet.
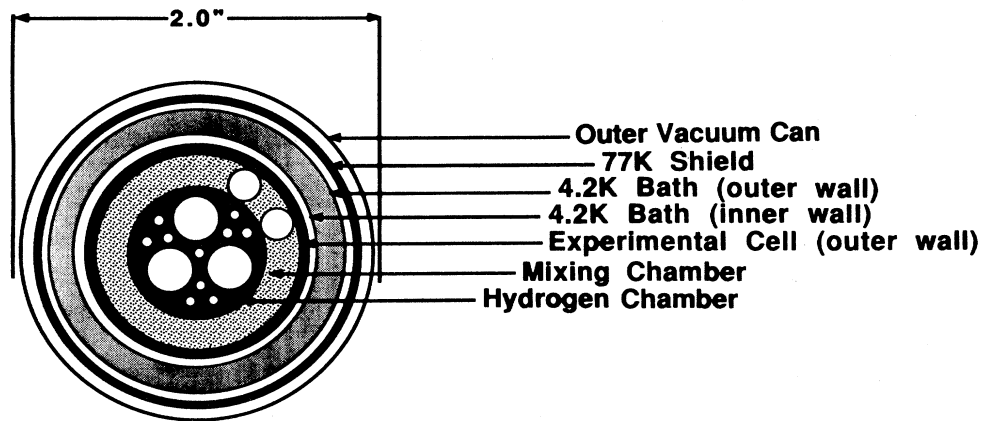
FIG. 2. Cross-sectional view of cryostat tailpiece in the region of the sample cell in the center of the field. The small holes carry bundles of copper wires used for thermal contact between the mixing chamber and the hydrogen compression chamber.

0.5-K radiation shield to gain some extra working space in the tail pieces.

The refrigerator is suspended above the magnet and lowered into place with a mechanical hoist. By sacrificing a few millimeters of radial dimension, we are able to suspend the refrigerator inside the magnet without touching the bore walls, thereby isolating the experiment from direct vibration from the magnet itself.

D. The compression cell

The hydrogen compression cell is constructed out of Stycast 1266 epoxy to avoid eddy-current heating from the magnetic-field ripple (see the Appendix). The body of the cell was machined out of a solid cylinder of epoxy which we cast at room temperature and then annealed at 90 °C for 3 h to relieve internal stresses which may have built up during the exothermic curing process. After machining, the cell was reannealed for 3 h at 90 °C to relieve any additional internal stresses.

A great number of fine copper wires were strategically imbedded in the cell in a geometry which breaks up the eddy currents while allowing good thermal conduction between the mixing chamber and the hydrogen compression chamber. After the final stage of assembly, the completed cell was once again annealed at 90 °C for 3 h to relieve any final internal stresses. The cell is shown in cross section schematically in Fig. 3. The various components of the cell are described separately below. Italicized terms are pointed out in Fig. 3.

The mixing chamber is a cylindrical annular cavity of about 6 ml volume which is built into the compression cell in order to maintain close proximity to the hydrogen sample. It contains a heater made from a 100-Ω metal-film resistor for positive feedback in a temperature-regulation circuit. The copper filaments (not shown in figure) which form the thermal link between the mixing chamber and the hydrogen sample are composed of very pure copper (with a measured residual resistivity ratio of 137) for good conduction at low temperatures. A chemical coating (Enthone-C) was applied to the 75-μm-diam. filaments to serve as an insulator to prevent electrical

cross conduction and further reduce eddy-current heating. As the filaments enter the mixing chamber, they fan out and are stripped of their insulation to provide a large clean surface area for reduced Kapitza resistance. The other end of the filaments which extend into the hydrogen space are fused into a solid disk of copper which
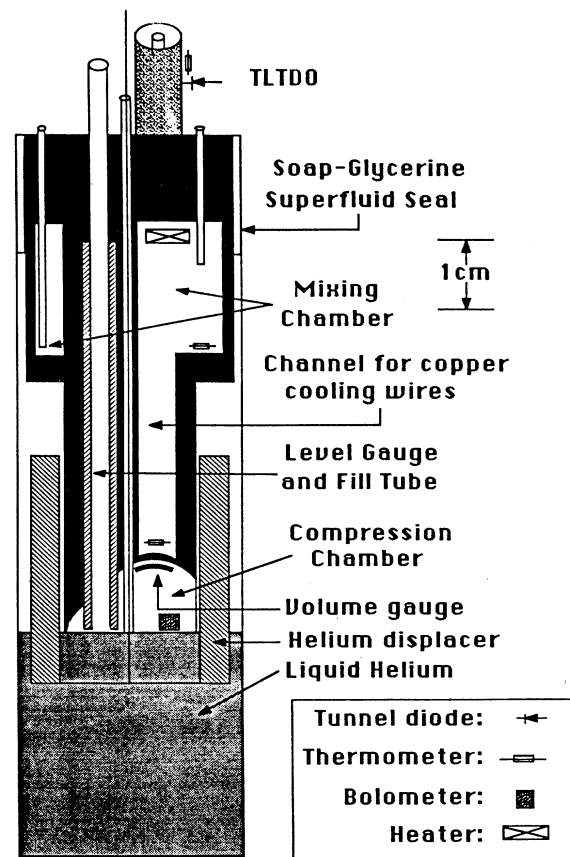

FIG. 3. Cut-away view of the experimental cell. The various components are described in the text.

forms the upper capacitor plate of the volume gauge (described below). The lower capacitor plate is similarly fused from fine copper filaments (not shown) which extend downward into the compression space to be cooled by the liquid helium. Imbedded in the filaments immediately above the upper capacitor plate of the volume gauge is a Matsushita carbon *thermometer* (HML1). Imbedded in the inner wall of the mixing chamber is a cobalt nuclear-orientation thermometer, and another carbon resistance thermometer (HML2). In addition to the main cooling filament which is formed into the upper plate of the volume gauge, there are a number of smaller filament bundles which extend from the mixing chamber down into the compression chamber.

The *compression chamber* extends up to room temperature through the *hydrogen fill tube*. The upper part of the fill line is described in detail in subsection E below. The lower end of the fill line terminates in a *level gauge* which measures the height of the liquid-helium compression fluid in the cell. In order to make optimum use of the limited space available, the level gauge doubles as an extension of the fill tube and is used to load hydrogen atoms into the compression chamber. The level gauge is a split-cylinder capacitive sensor which is shown schematically in Fig. 4. The gauge is made of 1266 epoxy, plated with gold inside the bore to form two opposing electrodes. The two halves of the cylinder are held separate by a thin piece of cigarette paper, saturated in epoxy. The exterior is plated with gold to form a electromagnetic shield for use with a three-terminal capacitance bridge.

The *volume gauge* is a capacitive sensor which is formed by two circular copper plates 0.200 in. in diameter separated a distance of 0.53 mm by three small epoxy spacers. The plates were glued together under pressure using a custom x-y-z stage to facilitate proper alignment. The surfaces of the capacitor plates were precisely machined to have a slight spherical curvature of 0.5-in. radius to match the curved upper portion of the compression chamber. The inner surfaces of the capacitor plates were electropolished, silver plated, and then coated with 120 mg of a 1-μm-diameter silver sinter to reduce Kapitza resistance. The sinter was compressed in a jig under spring tension and baked in vacuum at 200 °C for 40 min. After sintering, the plates were resurfaced with an electrospark discharge machine. The electrospark machining usually takes place under a flowing bath of oil; however, to avoid clogging the sinter pores, we constructed a small flow chamber which used distilled and deionized water instead of oil. Finally, the plates were lightly etched with dilute nitric acid to ensure that the sinter pores were open. The acid etchant was rinsed out in an ultrasonic bath of distilled water, neutralized with NH_4OH, and rerinsed for an extended period. Phase-contrast microscopy was used to visually inspect the sinter pore structure after all the construction steps were complete. The upper capacitor plate is grounded and the lower plate is connected through an electrical feed through in the top of the compression chamber to the *transmission-line tunnel-diode oscillator* (TLTDO).[20]

The TLTDO is made of a 30 cm length of semirigid co-axial line modified for low temperature use in a Bitter magnet. To suppress eddy-current heating, the central copper conductor was chemically etched down to a thin layer and the outer conductor was made of stainless-steel plated on the inside with several skin depths of silver. The oscillator was tuned with a low-loss microwave capacitor to operate at over 200 MHz, allowing rapid time resolution in our measurements. Power is supplied by a *tunnel diode* which is dc biased from a nearby circuit, pinned at 4.2 K to reduce the heat load on the refrigerator. The oscillation is monitored by tapping off a small fraction of the oscillating current with a low-loss coaxial line which runs up to room temperature, through a filter-
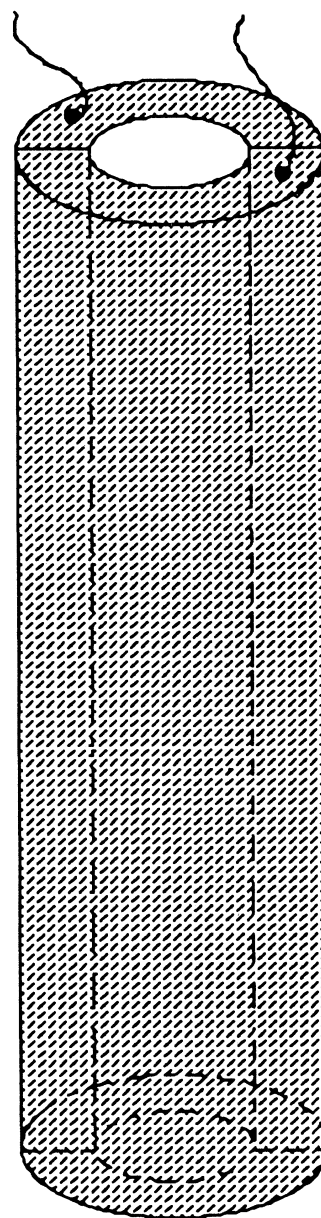

FIG. 4. The capacitive helium level gauge used to monitor the hydrostatic pressure.

ing and high-gain amplification network, and into a computer-controlled microwave-frequency counter.

The *helium displacer* is an annular cylindrical solid attached to a semirigid wire which runs up a tube through the center of the cell to room temperature. At the top of the cryostat, the wire is attached to a Burleigh model CE-2000 "inchworm" piezoelectric linear translator which operates through a sliding O-ring seal to move the displacer up and down several centimeters in the cell. The motion of the wire is microprocessor controlled and precisely monitored by a small optical interferometer mounted on the inchworm. The tube which carries the displacer wire to the cell has thermal pinning points at the refrigerator's 4.2-K bath, the 1.2-K pot, and the spiral heat exchanger, all to relieve the heat load on the cell from conduction from room temperature and from the refluxing superfluid film which normally exists in this tube when the compression chamber is filled with liquid helium.

A stainless-steel and Kapton-diaphragm pressure gauge is mounted on the hydrogen fill line immediately above the top of the cell. The pressure gauge is monitored at room temperature with a General Radio (GR) capacitance bridge. A carbon thermometer is mounted directly on the pressure gauge to monitor its temperature.

A pair of *trigger bolometers*[7] made from carbon resistor chips are suspended in the compression chamber by thin wires and used as a sensitive detector of hydrogen atoms. The bolometers are normally coated with a layer of superfluid helium, but when heated with an electrical current, they boil off the helium faster than it can be replenished by flowing down the thin wires. Once bare of the protective helium coating, hydrogen atoms rapidly recombine on the uncovered surface and lead to explosive recombination. Such an explosion puts a thermal pulse on the bolometer which can then be detected by monitoring the temperature-dependent resistance of the bolometer itself. These bolometers are useful in optimizing the filling flux of H atoms from the discharge.

The compression chamber and measuring devices are accessible through a removable epoxy jacket which forms the outer wall of the helium compression-fluid reservoir. The jacket is secured in place with a *soap-Glycerine seal*[21] at the top of the cell, just below the diaphragm pressure gauge.

In all, there are five stainless-steel tubes which exit the top of the cell (Fig. 2): The fill tube, the oscillator transmission line, the displacer-tube, and the two circulation lines to the mixing chamber. In addition, there are a number of channels containing cooling braids which extend downward between the mixing chamber to the compression chamber. To guard against cracking induced by the thermal expansion mismatch between the metal tubes and the epoxy cell body, all of the tube walls were thinned down to ≤ 0.005-in. thickness where they enter the cell body to allow flexure under compression.

E. The hydrogen-inlet system

Atoms are transported from room temperature to the cryogenic environment of the compression chamber via the hydrogen-inlet system (Fig. 5). In the first step, high-purity molecular hydrogen is fed through a liquid-nitrogen-cooled trap in a gas-handling system and into a microwave-discharge cavity[22] located directly on top of the dilution refrigerator. The discharge is operated at about 1 Torr of pressure and is driven by 20–30 W of power at 2.4 GHz. The fringing fields at the end of the discharge cavity dissociate the hydrogen molecules into atomic constituents, which then diffuse through an orifice and a Teflon valve into the cryostat. All surfaces between the discharge and the low-temperature environment are coated with teflon to prevent the hydrogen atoms from sticking to the surface where they can recombine rapidly.

The upper section of the fill line extends through the main helium bath of the refrigerator via a double-walled tube. The inner wall of the tube is wound with an electrical heater to warm the Teflon enough to keep it effective in preventing surface recombination. This section of the fill tube contains five silicon diode thermometers to monitor the temperature profile.

Just before the fill tube enters the "1.2-K-pot" region of the refrigerator it is weakly pinned to the main bath at 4.2 K. This pinning point is called the thermal "accommodator;" it is the first stage in what will be a rapid cool-down to less than 0.9 K over a distance of less than
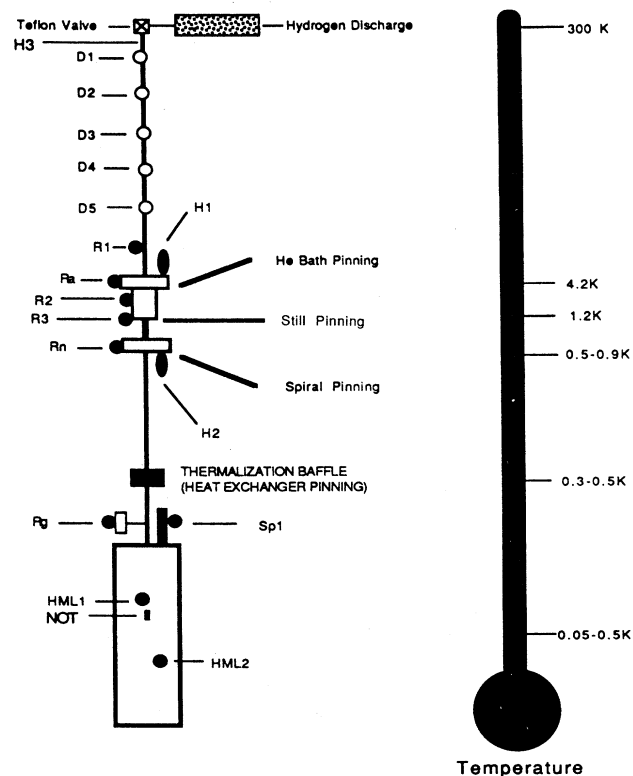

FIG. 5. Schematic diagram of the hydrogen-inlet system. The D's indicate silicon diode thermometers; carbon-resistance thermometers are indicated by R, HML, and Sp; NOT is a nuclear orientation thermometer; H indicates heater. The distance from top to bottom is about two meters.

3 in. It is essential that the distance between 4 and 0.9 K be kept very short since atoms rapidly recombine on the surface in this region. Below about 0.9 K, the surface can sustain a film of superfluid helium which greatly suppresses recombination.

Below the accommodator, the fill tube is pinned to the still, where it is necked down to a smaller diameter to limit film flow. About an inch lower, the fill tube is pinned to the spiral heat exchanger which normally runs at about 0.5 K. This region is called the "HEVAC" (Ref. 7) for historical reasons. The HEVAC and the accommodator each have their own wire wound heaters to adjust their temperatures. In addition, there are five carbon thermometers strung along the short distance between the accommodator and the HEVAC. Numerous modifications to the HEVAC-accommodator region had to be made to find an optimum configuration which did not overload the refrigerator while still providing an adequate temperature gradient and geometry to allow successful transport of atoms through this region.

Between the HEVAC and the cell, a baffle is inserted into the fill tube and pinned to the lowest heat exchanger to insure adequate precooling of the hydrogen before entering the compression chamber. With the apparatus described in this section, hydrogen can be successfully loaded into the cell in preparation for data collection, as described in the next section. However, in all of our measurements, the most serious continuing problem was the limited cooling power of the refrigerator which was marginally adequate and usually resulted in low initial densities of H↓.

III. DATA COLLECTION

A. Procedure

At the beginning of an experiment, the displacer (Fig. 3) is lowered to the bottom of the cell and the cell is filled with liquid ^{4}He up to a distance of several millimeters above the top of the volume gauge. The displacer is then raised up out of the ^{4}He until the level drops below the lower end of the level gauge. Atomic hydrogen can then flow down the fill line from the room-temperature dissociator and enter the precompression space [Fig. 6(a)]. When a significant number of atoms have accumulated in the precompression space, the displacer is lowered, raising the ^{4}He level until the lower end of the level gauge is sealed off. As the level is further raised, the hydrogen gas is compressed into an increasingly smaller volume, raising the density. The spherically curved roof of the precompression space forces the hydrogen to eventually end up as a small bubble squeezed between the capacitor plates of the volume gauge [Fig. 6(b)]. The motion of the displacer is then stopped and held constant, allowing the hydrogen atoms to decay under fixed hydrostatic pressure and temperature. As the H↓ atoms decay, the volume of helium displaced from between the capacitor plates is reduced and the capacitance changes due to the finite dielectric constant of the liquid helium. Changes in the capacitance are monitored by the TLTDO circuit mounted directly on the top of the cell.
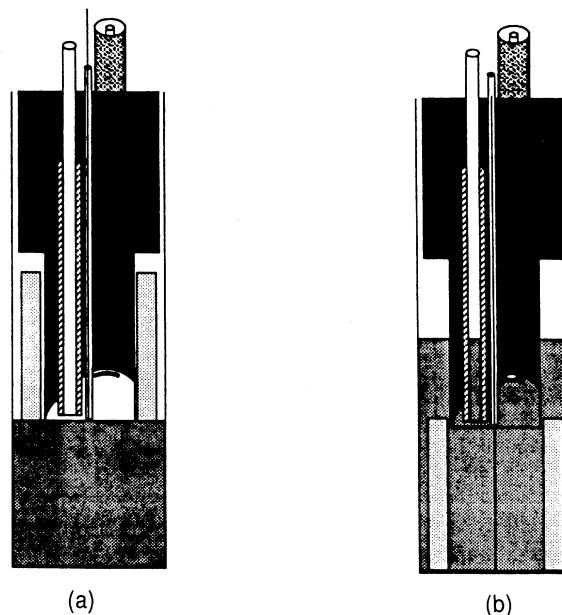

(a)   (b)

FIG. 6. The compression sequence. (a) With He level low, the cell is filled with hydrogen atoms through the level gauge. (b) The He level is raised, compressing the hydrogen atoms between the capacitor plates of the volume gauge.

Data from the TLTDO frequency counter are collected and stored directly with a desk-top personal computer (PC), via an IEEE bus. The level gauge is monitored with a general radio capacitance bridge connected to an external lock-in amplifier; the amplifier output is fed through an analog-to-digital converter (ADC) and into the PC. The cell thermometer is monitored with a resistance bridge and regulated with a temperature controller operating on the mixing-chamber heater; the bridge balance signal is fed through the ADC and into the PC for reference. The data are later transferred via modem from the PC at the FBNML lab to our VAX computer at Harvard for analysis.

B. Volume decay and oscillation

Some data showing a bubble decaying at 20 T are presented in Fig. 7. We have sometimes observed that a decaying bubble will appear to spontaneously undergo pronounced oscillations in volume. Similar oscillations were observed in the experiment by Sprik et al.[1,2] Tommila, et al., also reported oscillations immediately after compression;[4] however, these may have been of a fundamentally different nature. We did not use any of the data in regions of oscillation for the analysis described in this paper, however, we describe them in some detail below.

The oscillations shown in Fig. 8(a) are among the most pronounced and clearly resolved that we have observed. These data were taken under conditions of unusually low magnetic field strength ($B < 5$ T) when we were prevented from accessing higher fields due to a technical problem with the magnet. The oscillations grow steadily in ampli-
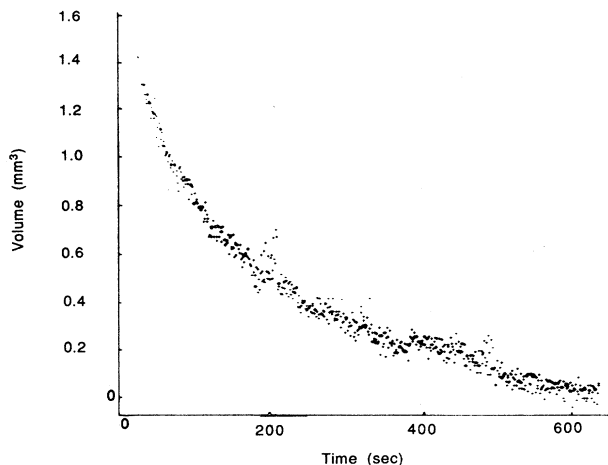
FIG. 7. Response of the volume gauge, showing temporal decay of hydrogen at 20 T.

FIG. 8. (a) A decay curve with an oscillation. (b) Expanded view of the oscillation.

tude and sometimes, remarkably, damp out almost discontinuously. At other times, the oscillations can terminate in explosion of the bubble. It is unclear whether the oscillations are warming the gas to the explosion limit or if an already overheated gas is driving the oscillations. The oscillations are asymetric about the quiescent level, occurring predominantly in the direction of increasing volume. The period of the oscillations shown in Fig. 8(b) are about 5 sec from peak to trough. We have observed oscillations with shorter periods at higher fields, though we have not systematically studied them.

The oscillation cannot be explained by a simple consideration of cavitation modes, for which the frequency of oscillation is given by[23]

$$ \nu_b = \frac{1}{2\pi} \left[\frac{4\gamma}{\rho R^3} \right]^{1/2} . \tag{1} $$

Upon inserting the proper values for the surface tension (γ) and bulk density (ρ) of liquid helium, Eq. (1) does not come close to predicting the observed frequency of oscillation [Eq. (1) predicts $\nu_b = 16$ Hz for a 1-mm-radius bubble].

A more realistic approach would include the recombination heating in the equations for cavitation oscillations. If, in a fluctuation, the density was increased, the recombination heat from three-body decay would also increase rapidly (as the cube of the density). This might overheat the gas and cause the bubble to expand. The expansion would reduce the heating and feedback to cool the bubble, which then contracts. Then the cycle would start over again. At low temperatures where heating is limited by surface decay with a very strong (exponential) temperature dependence, the feedback mechanism might be very strong in suppressing oscillations.

C. Device calibrations

Before the raw data can be properly interpreted, a number of measuring devices in the cell must be calibrat-
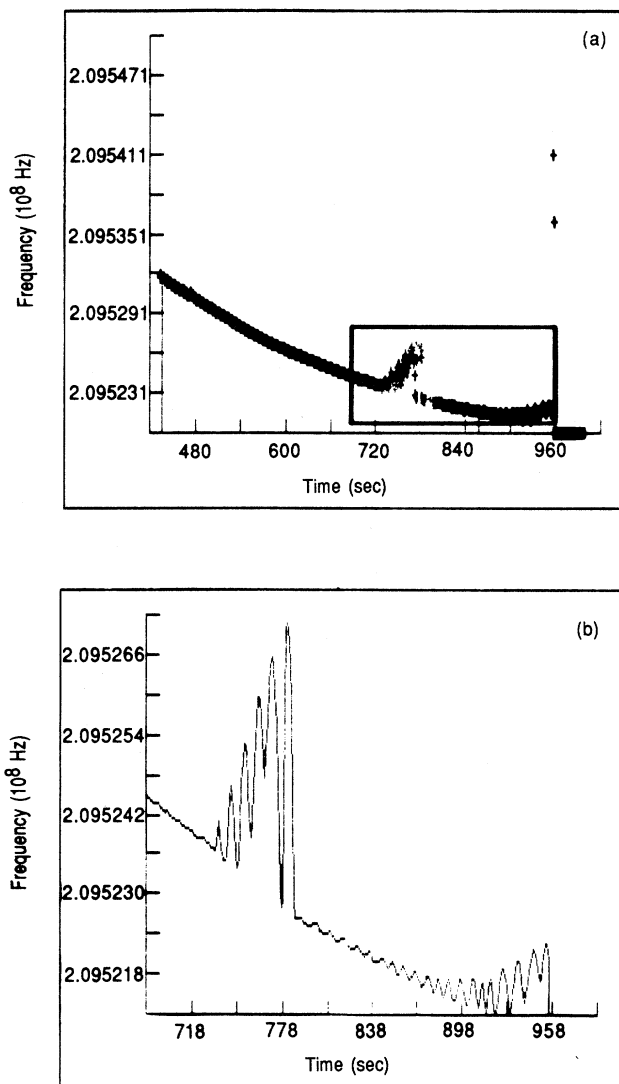
ed. All of the measuring devices were calibrated *in situ* at low temperature—a procedure which is essential for accurate results. The calibration procedures are described separately below.

(i) *Level-gauge calibration.* Two independent methods were used to calibrate the level gauge; this provided a cross check for possible systematic errors in either of the methods.

First, the cell was loaded with an excess of liquid ^{4}He so as to completely fill the level gauge. The measured change in capacitance along with the known length of the gauge gives a calibration factor: $dL/dC = 612$ mm/pF. Using this factor to measure small deviations in the level near the middle of the gauge rests on the assumption that the fringing fields at the ends of the gauge contribute little to the total capacitance, and that the gauge is uniform along its length.

Second, the level gauge was calibrated directly for small excursions in the ^{4}He level near the center of the gauge by moving the displacer by a measured amount. The corresponding change in the height of the helium was determined by the well-known dimensions of the cell geometry in the region of interest (just above the top of the upper plate of the volume gauge, the cross section of the cell consists of a simple geometry, with all surfaces circular in outline). The displacement of the plunger is measured with great precision by the optical encoder on the inchworm translator. Uncertainty in the displacement of the helium is likely to be limited by the lack of absolute rigidity of the connecting wire which links the plunger to the inchworm. This method yielded a calibration factor: $dL/dC = 609$ mm/pF, in agreement with the previous method to within 0.5%. Based on the above results, we take a value, $dL/dC = 609$ mm/pF to analyze the data. This value was rechecked several times throughout the course of the data collection to ensure against unexpected shifts in the calibration.

In addition to the calibration factor (dL/dC), we use the known weight of liquid helium to determine the hydrostatic pressure (1.42 Pa/mm ^{4}He). Because the hydrostatic pressures used in this experiment were significantly smaller and our magnet homogeneity was significantly greater than those used in previous studies, the diamagnetic interaction of the helium with field gradients near the center of the field maximum reduces the total pressure by only a few percent, which we neglect.

To obtain an absolute value for the hydrostatic pressure it is necessary to determine the zero of the pressure reading. A naive estimate for this can be obtained by slowly sweeping the helium level upwards without hydrogen atoms in the cell and noting the position of the level gauge at which the volume gauge stops responding; this corresponds to the point at which the helium compression fluid rises above the plates of the volume gauge. Capillarity effects in the compression chamber and the level gauge can result in an offset from the true hydrostatic pressure reading using this method. Such an offset ($\Delta P = -2.2$ Pa) was corrected for directly by measuring the compressibility of a hydrogen bubble at low density and requiring the results to conform to the ideal gas law. A crude calculation of the expected offset agrees to within 20% of the observed offset. This technique was used previously by Tommila et al.[4] to obtain a precise zero for their level gauge also. Long term drift was eliminated by redetermining the zero at the beginning of each run. Short-term drift is corrected for by comparing the initial values of the level gauge capacitance when the helium level is lowered below the end of the level gauge. The capillary offset should depend only on cell geometry, and in fact is not observed to vary from run to run.

(ii) Volume-gauge calibration. Although measurements of the volume form our principal data, an absolute calibration of the volume gauge is much less crucial for extracting the recombination rate constants than one might naively expect. As will be seen in detail below, the expression for the temporal decay of the volume can be factored and rewritten in terms of the inverse decay time, $(1/V)(dV/dt')$ so that, to this extent, the volume can remain indeterminate up to a constant multiplicative scale factor. The absolute value of the volume enters directly in more subtle but less crucial ways. For example, the absolute volume effects the pressure inside the bubble via the surface tension, but this contribution scales rather weakly with the volume [e.g., $P \sim (1/V)^{1/3}$ for a spherical bubble with no hydrostatic pressure].

By tracking small changes in the oscillator frequency (ν), we monitor changes in the capacitance (C) of the volume gauge which can be related to the volume (V) of the hydrogen bubble. In general, we can write the response of the circuit as a Taylor expansion,

$$\nu = f(C(V)) = \nu_{0+}\alpha V + \cdots . \qquad (2)$$

ν_0 is determined by the base line obtained after each bubble decays to zero volume. The low dielectric constant of helium ($\epsilon_r = 1.057$) (Ref. 1) results in very small changes in TLDO frequency as helium is displaced, and hence the linearization of the above expansion is very accurate. Shape-dependent demagnetization factors are also reduced to negligible importance because of the low dielectric constant of the helium, as shown by Sprik.[2]

To guard against possible unsuspected systematic errors, the volume gauge calibration factor (α) was determined using two independent methods. Both methods involve measuring the change in the TLDO frequency as the helium level is slowly raised above the plates of the volume gauge. As the helium begins to fill the space between the plates the TLDO begins to change rapidly. Dividing the measured change in TLDO frequency as the plates fill with helium by the known volume between the plates results in a calibration factor of: $\alpha \lesssim 19$ KHz/mm^3. Significant stray capacitance and fringing fields in the highly compact cell make an accurate determination of the calibration factor difficult since the TLDO responds to the rising helium even with the helium level well below the plates of the volume gauge.

We have used a second method of calibrating the volume gauge which greatly reduces the uncertainty associated with the fringing fields by incorporating them into a direct measurement of the total capacitance (C) and the plate spacing (d) of the volume gauge. The entire capacitance of the volume gauge (volume-gauge plates, plus stray) is measured with a GR bridge before cooling down the cell. The bridge is replaced by the tunnel-diode circuit, the cell is cooled, and the sensitivity is determined by filling the cell with enough helium to cover the plates of the volume gauge entirely and noting the corresponding change in TLDO frequency ($\Delta \nu_{tot}$) which occurs at low temperature. To within the uncertainty which results from changes upon cooling, one can determine the volume (V) of a small bubble in the helium by using the following result (cf. Sprik[2]):

$$V = \left[\frac{\epsilon_r C d^2}{\epsilon_0 (\epsilon_r - 1)} \right] \frac{\Delta \nu}{\Delta \nu_{tot}} . \qquad (3)$$

This method is much less sensitive to fringing fields because Eq. (3) assumes only that the electric field lines are parallel at the center of the capacitor plates where the bubble resides. The effect of the fringing fields is incor-

porated into the direct measurement of the total capacitance and the sampling of the fringing fields by the helium as it is raised to cover the entire volume gauge. The result for the volume-gauge calibration factor using this method is 16 KHz/mm^3, in reasonable agreement with the upper bound determined by the previous method. We use this latter value for the analysis of our data.

(iii) *Thermometer calibration*. The apparatus contains 15 thermometers, strategically located to characterize all components of the system. The thermometer which was used to determine the temperature of the decaying hydrogen sample, HML1, was calibrated *in situ* using the ^{3}He vapor pressure scale.[24] Magnetoresistance was also measured *in situ* for fields up to 20 T. The vapor pressure was monitored by the pressure gauge located on the fill tube just above the cell, as well as by a room temperature Barocell manometer. Room-temperature pressures were corrected for the thermomolecular effect.[25] For temperatures 500 mK and higher the thermomolecular correction to the pressure is less than 5% corresponding to a correction to the temperature of less than 1%. Since the thermomolecular effect depends on the radius of the connecting tube, we could directly check the small nature of the effect by alternating measurements between the (large diameter) fill tube and the (small diameter) displacer line. We believe that an absolute calibration of our thermometers is accurate to better than 5% in the range of interest.

Note that the calibration discussed in this section was performed *after* the measurements were taken (except 17-T data). This insured that the ^{4}He compression fluid was not contaminated by ^{3}He atoms. Even small amounts of ^{3}He in the compression fluid can radically alter the adsorption energy and thus interfere with a proper determination of the decay rates.[26] The cell was pumped out thoroughly and kept at room temperature for many weeks before cooling down again to take the 17-T data, so contamination should not be a problem with the 17-T data either. In addition, we began with 99.999% pure ^{4}He and condensed in through a liquid-nitrogen trap. The displacer line serves as an *in situ* liquid-helium trap for the fluid before it enters the cell.

IV. DATA ANALYSIS

A. The rate equations

Spin-polarized atomic hydrogen in a high-magnetic field is composed of two nearly degenerate states (the a and b states shown in Fig. 9) which nevertheless decay at very different rates because of the remnant hyperfine mixing in a-state atoms. To properly model the temporal decay of the volume (V), therefore, one must keep track of the density of a state atoms ($n_a = N_a / V$) and the density of b state atoms ($n_b = N_b / V$) separately,

$$\frac{1}{V}\frac{dV}{dt} = \left[\frac{dN_a}{dt} + \frac{dN_b}{dt}\right]\frac{1}{N_a + N_b}\frac{1}{\mathcal{C}(V,P)} . \quad (4)$$

The function $\mathcal{C}(V,P)$ accounts for the changing total pressure due to the size-dependent surface tension contribution to the pressure (P_γ),
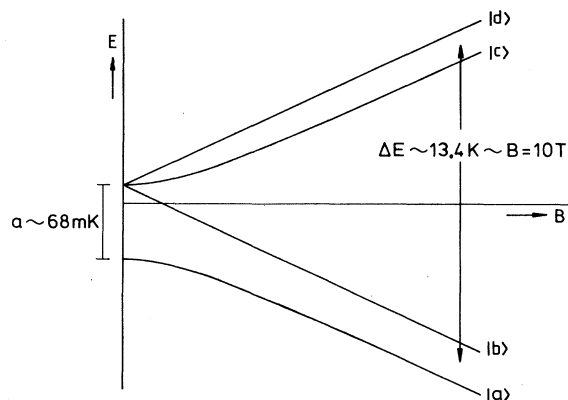

FIG. 9. The four hyperfine energy levels of atomic hydrogen in a magnetic field.

$$P = P_{\text{hydrostatic}} + P_\gamma(V) . \quad (5)$$

The specific form of the function $P_\gamma(V)$ for our geometry is discussed below. The expression for $\mathcal{C}(V,P)$ is found by direct differentiation of the ideal-gas equation of state, which accurately describes spin-polarized atomic hydrogen at these densities and temperatures,

$$\mathcal{C}(V,P) = \left[1 + \frac{V}{P}\frac{dP}{dV}\right] . \quad (6)$$

We now discuss the form of the function $P_\gamma(V)$. In our apparatus, the hydrogen sample consists of a pancake-shaped bubble squeezed between the plates of the volume gauge (Fig. 10). The slight curvature of the volume-gauge plates can be neglected for the purpose of this calculation. Following Tommila *et al.*,[4] we approximate the pancake shape by assuming that the meniscus has a semicircular profile. In this case the A/V ratio and the volume-dependent surface-tension contribution to the pressure needed in the above equations can be written in closed form using the expressions,

$$V = 2\pi R^2 r + \tfrac{4}{3}\pi r^3 + \pi^2 R r^2 ,$$
$$A = 2\pi R^2 + 2\pi^2 R r + 4\pi r^2 . \quad (7)$$

The small radius of curvature (r) is determined by the plate separation (h) of the volume gauge, $r = h/2 = 0.27$ mm. If we reference the hydrostatic pressure from the
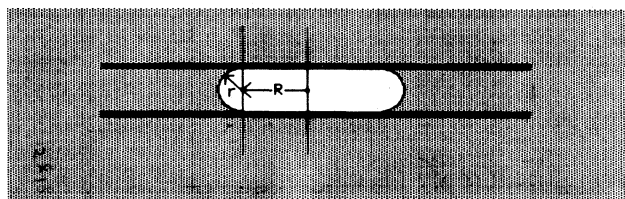

FIG. 10. The pancake geometry of the hydrogen bubble.

upper capacitor plate, then $P_\gamma(V)$ is given by

$$P_\gamma(V) = \gamma \left[\frac{1}{r} + \frac{1}{R+r} \right] + \rho g r \ . \tag{8}$$

The last term is the hydrostatic pressure between the upper plate and the midplane of the plates (ρ=density of helium=0.145 g/cm^3, g=980 cm/sec^2). The other terms give the interfacial pressure jump between the hydrogen gas and the bulk helium at the midplane as given by the Young-Laplace equation.[1] We have used γ=0.378 ergs cm^{-2} for the value of the surface tension of ^{4}He.[27]

The decay of the a- and b-state atoms is modeled in the usual way,[28] keeping track of the relevant relaxation and recombination processes for our range of magnetic field and temperature,

$$\frac{1}{V} \frac{dN_a}{dt} = -(2+\xi\eta)\dot{r}_a - \xi\eta(\dot{r}_a+\dot{r}_b)[n_a/(n_a+n_b)]$$
$$- 2K_{aa}^{\text{eff}}n_a^2 - K_{ab}^{\text{eff}}n_a n_b - G_{ab}^{\text{eff}}(n_a+n_b)(n_a-n_b)$$
$$- C_{\text{ex}}(\tfrac{8}{3}n_a^3 + \tfrac{4}{9}n_b n_a^2) - \tfrac{2}{3}\xi\eta K_{bbb}(n_b-n_a)n_a n_b \ ,$$
$$\tag{9}$$
$$\frac{1}{V} \frac{dN_b}{dt} = -(2+\xi\eta)\dot{r}_b - \xi\eta(\dot{r}_a+\dot{r}_b)[n_b/(n_a+n_b)]$$
$$- K_{ab}^{\text{eff}}n_a n_b + G_{ab}^{\text{eff}}(n_a+n_b)(n_a-n_b)$$
$$- C_{\text{ex}}(\tfrac{2}{9}n_b n_a^2 - \tfrac{2}{3}n_a^3) + \tfrac{2}{3}\xi\eta K_{bbb}(n_b-n_a)n_a n_b \ ,$$

with

$$\dot{r}_a = K_{bbb}(n_a^3 + \tfrac{2}{3}n_b n_a^2 + \tfrac{1}{3}n_a n_b^2) \ ,$$
$$\dot{r}_b = K_{bbb}(n_b^3 + \tfrac{1}{3}n_b n_a^2 + \tfrac{2}{3}n_a n_b^2) \ . \tag{10}$$

In these equations, the rate constants denoted by K_{ij} (the subscripts $i,j \in [a,b]$ denote initial hyperfine states of atoms in a collision event) represent two-body exchange recombination processes which occur on the surface of the hydrogen bubble. Rate constants denoted with a G represent dipole-dipole relaxation processes which occur both in the bulk and on the surface. Rate constants denoted with a C_{ex} refer to three-body exchange recombination. Rate constants denoted by K_{bbb} represent three-body dipolar recombination. The constant ξ denotes the fraction of three-body dipolar events which proceed via the double-spin-flip (DSF) channel, and the constant η accounts for the fraction of DSF events $(1-\eta)$ which subsequently relax back down to the a or b state from the c or d state before recombining. The first three-body dipolar term which occurs in Eqs. (9), $(2+\xi\eta)\dot{r}_i$, accounts for atoms which are lost immediately during the collision process. The following term accounts for subsequent loss of c- and d-state atoms which are generated by the DSF dipolar channel; here it is assumed that the probability of a c- or d-state atom recombining with an a- or a b-state atom is directly proportional to the fraction of a- or b-state atoms, respectively. The last term in Eqs. (9) accounts for the rapid spin-exchange relaxation which occurs immediately after a DSF event; this term is included for completeness but is not very significant for analyzing the data (a similar term was implicit in the equations used by Bell et al.[3]). The derivation of the expressions for $\dot{r}_a$ and $\dot{r}_b$ is discussed by Silvera and Walraven.[28] Rate constants denoted with a superscript "eff" represent effective rate constants which account for both surface (subscript s) and bulk (subscript V) events where appropriate,

$$X^{\text{eff}} = X_V + X_s \frac{A}{V}(\lambda(T)e^{E_b/kT})^n \ . \tag{11}$$

In this expression the value of n represents the number of hydrogen atoms involved in the recombination-relaxation process, and E_b is the adsorption energy for atomic hydrogen in ^{4}He.

Combining the expression (9) and (10) for $N = N_a + N_b$ we can write the three-body dipolar contributions to the decay in terms of an effective rate constant (L^{eff}),

$$\frac{dN}{dt} = L^{\text{eff}}n^3 f_3(\hat{a}) \ , \tag{12}$$

with,

$$L^{\text{eff}} = 2(1+\xi\eta)K_{bbb} \ ,$$
$$f_3(\hat{a}) = (1+\hat{a}+\hat{a}^2+\hat{a}^3)/(1+\hat{a})^3 \ , \tag{13}$$
$$\hat{a} = N_a/N_b \ .$$

We will express the final results of our fits to the data in terms of L^{eff} and C_{ex}.

B. Fitting procedure

Starting with an initial volume given by the raw data, the above coupled differential equations are numerically integrated to give a theoretical decay curve. Each of the raw data points is equally weighted and used to determine a value of χ^2 in reference to the simulated decay. χ^2 is then minimized by varying three parameters in the simulation: The initial polarization ratio (N_a/N_b), the three-body dipole rate constant, and the three-body-exchange rate constant. The STEPIT algorithm[29] was used to locate the minimum of the χ^2 surface. A fourth-order Runge-Kutta[30] numerical procedure was used to integrate the rate equations. The 1σ statistical errors are determined for the equally weighted raw data by finding the amount which a given parameter must be varied to make chi-square increase from a best-fit value of one to a maximum value of two. It is important in determining the 1σ limits for any given parameter that the other free parameters be allowed to readjust themselves to keep χ^2 minimized. Failure to allow for this readjustment would underestimate the true 1σ uncertainties since the fit parameters are correlated variables.

Table I lists the values of the fundamental parameters assumed known for this analysis. We point out that the field dependence shown for the *two-body* recombination and relaxation parameters is that predicted by theory and confirmed by experiments for fields below 10 T. It is assumed that the theoretically predicted two-body field dependence is valid up to 20 T.

An early publication of our preliminary results[31] used the "asymptotic polarization method" of analysis used in

TABLE I. Constants used in analyzing the data in this work. The factors ξ were taken from Ref. 28 and η was estimated using the expression in Ref. 1. For the above expressions, B is in T and T in Kelvin.

$K_{ab} = (3.3 \times 10^{-8})B^{-2}\sqrt{T}$ (cm^2/sec)	35
$\gamma = K_{aa}/K_{ab} = 2.5$	35
$\epsilon_b = 0.96$ (K)	35
$G_v = (6.9 \times 10^{-22})(1 + 16.68/B)^2\sqrt{T}$ (cm^3/sec)	1
$G_s = (1 + 16.68/B)^2(0.69 - 0.45T + 0.52T^2) \times 10^{-14}$ (cm^2/sec)	36
$\xi\eta = 0.73$ (for $B \leq 15T$, $T = 500$ mK)	
$\xi\eta = 0.66$ (for $B = 17T$, $T = 500$ mK)	
$\xi\eta = 0.63$ (for $B = 20T$, $T = 500$ mK)	

some previous experiments,[1,3] and showed the same general conclusions which are presented here. However, since this preliminary analysis was more susceptible to systematic error in the form of insufficient buildup of nuclear polarization, we use the more sophisticated fitting procedure described here for our final determination of the rate constants. A fitting procedure similar to the one used here has also been used by other groups.[3,4] This method of analysis was particularly appropriate for our data because our very low filling flux and limited magnet time resulted in low initial densities which ultimately translated into low initial nuclear polarization values and limited dynamic range in the volume decay.

C. Results

The results of analyzing the decays are shown individually in Fig. 11. Although the data are very noisy, they seem to show a systematic dependence on magnetic field strength. In order to avoid subjective bias in selecting the "good data" from the "bad data" and in order to make optimal use of the few acceptable decays that we were able collect within the time constraints at the magnet laboratory, we implemented the procedure of careful-

ly determining the statistical error (1σ) associated with each fit as described above. We then performed a weighted average of the data collected at each field strength. The "bad data" (noisy, small dynamic range, etc.) naturally display a large statistical error without the need for subjective assessment. We performed the weighted average using standard Gaussian error statistics,[32]

$$\langle x \rangle = \langle \sigma \rangle^2 \sum_i \frac{x_i}{\sigma_i^2},$$

$$\sigma = \left[\sum_i \frac{1}{\sigma_i^2} \right]^{-1/2}. \tag{14}$$

The final results shown in Fig. 12 and Table II clearly display a peak near 15 T as predicted by theory.

Potential sources of systematic error in L due to our assumptions about the value of $\xi\eta$ were checked by refitting some curves for a variety of assumed values for $\xi\eta$. Even when $\xi\eta$ was allowed to vary over the entire physically allowed range of possibilities (0–1), the shift in L was only about 10%, demonstrating the insensitivity of the fits to our assumptions for $\xi\eta$.

The bulk three-body-recombination rate constants are predicted to be independent of temperature in the range under consideration. Most of the data were taken at 500
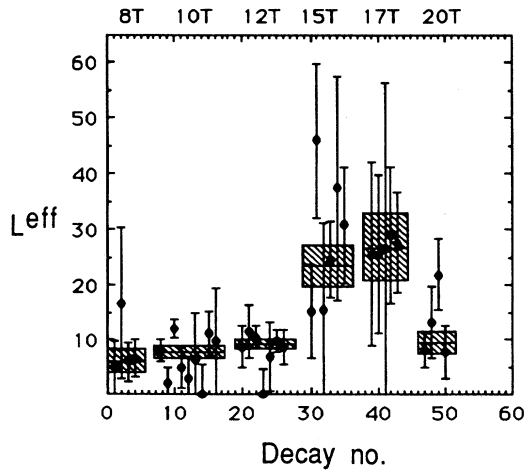

FIG. 11. Best fit values for the three-body decay rate constants for each individual decay curve (labeled by id. no.). Also shown as a cross-hatched bar for each field are the weighted mean plus or minus the weighted error as described in the text.
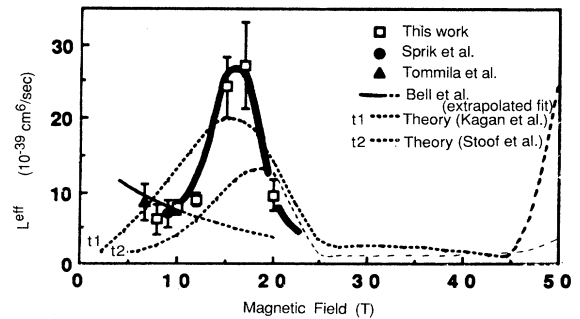

FIG. 12. Weighted mean values for the three-body dipolar recombination rate constant as a function of magnetic field up to 20 T. Also shown are some theoretical predictions and some measurements by other groups at fields below 10 T: Sprik *et al.* (Ref. 1), Tommila *et al.* (Ref. 4), Bell *et al.* (Ref. 3), Kagan *et al.* (Ref. 11), Stoof *et al.* (Ref. 15).

TABLE II. The tabular form of results plotted in Figs. 12 and 13. The numbers in parentheses give the standard deviation of the value.

B (T)	L_{eff} (10^{-39} cm^6/sec)	C_{ex} (10^{-39} cm^6/sec)
8	6.2 (2.1)	79 (180)
10	7.9 (1.0)	140 (120)
12	9.0 (1.0)	250 (93)
15	24 (4.1)	160 (200)
17	27 (6.0)	590 (640)
20	9.6 (2.1)	63 (370)

FIG. 13. The mean values for three-body exchange rate constants as a function of magnetic field. Data taken from Bell et al. (Ref. 3) and Kagan et al. (Ref. 11) as well as this work.

mK. Half the data at 15 and 20 T were taken at 545 mK, and showed no significant increase in the determined value of L, thereby supporting our assumption that we are in the bulk-dominated regime. The data at 8 T were taken at 600 mK in a superconducting magnet.

Quantitative agreement with the best available theories[15] is still discrepant by a factor of two. We have tried to eliminate all possible sources of systematic error from our data, and believe that any remaining systematics will contribute errors smaller than the statistical errors shown in Fig. 12; the data of 12 T may be an exception to this statement, where the average over a fairly large number of less noisy decays resulted in an unusually small statistical error.

Concerning the quantitative comparison between theory and experiment, we will make a few comments. First, one should keep in mind that we assume the three-body decay in our data is dominated by bulk processes. In fact, our data were not taken at quite the optimum temperature for measurement for pure bulk recombination. This circumstance arose, as mentioned above, because we waited until after the data were collected to do a precise ^{3}He vapor-pressure calibration of our thermometers to avoid the possibility of ^{3}He contamination of the adsorption energy. The previously measured[3] values at 8 T indicate that there may be as much as 16% contribution from the surface three-body decay. One cannot rule out the possibility that this fraction increases significantly as the magnetic field is increased. It is conceivable that the factor of two discrepancy between theory and experiment near the peak could be accounted for by a much increased surface contribution near 15 T. Theory[12,13] indicates that the surface and bulk contributions should both show the same *qualitative* behavior; however, the ratio of the two contributions is uncertain at this stage in the development of the theory. Ultimately, one would hope for a future experimental determination of the surface rates.

Before leaving the matter of surface decay, it should be pointed out that if one wanted to interpret our results for L_{eff} as the total rate including a possible contribution from the surface this would be only roughly correct and not absolutely rigorous since the area to volume ratio is changing somewhat during the course of a decay. A proper measurement of the total rate under such circumstances would have to separate out the surface and bulk contributions explicitly.
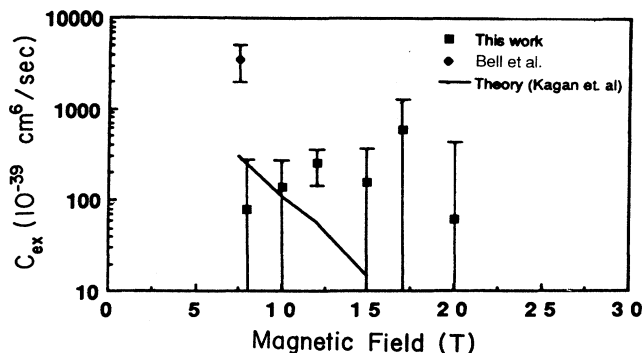
We should point out that the plot in Fig. 12 shows the

theoretical result in the limit $\eta = 1$, whereas, as discussed earlier, the results from the fit to the data made a first-order correction for the possibility of relaxation back down to the a or b states before recombination. The results of more recent calculations which present information necessary to estimate the effective rate constant for other values of η are forthcoming.[15] The correction for $\eta \neq 1$, however, should be less than 10%, as discussed above.

Our data for the three-body-exchange rate constant shown in Fig. 13 are consistent with the theory of Kagan et al.[11] and inconsistent with an earlier measurement by Bell et al.[3] who gave a value over an order of magnitude larger. Our measurements essentially put an upper bound on the exchange rate constant; higher precision measurements are needed to fully confirm the theory of Kagan et al.[11] Our bounds are important because the previously indicated much larger value for C_{ex} would have led to the conclusion that three-body exchange recombination could contribute significantly even for nuclear polarizations ($P \equiv (n_b - n_a)/(n_b + n_a)$) as high as 95%.

V. CONCLUSIONS

With the exchange rates now determined to be smaller and in better agreement with theory, we focus on the more important three-body dipolar recombination. Our data show for the time time the characteristic peak predicted near 15 T for the Kagan process. This novel feature results from the competition between field-dependent quantum interference in the overlap integrals and the reduction of final-state phase space as the double spin-flip cutoff field at 27 T is approached. Observation of this important qualitative feature confirms our faith in the underlying correctness of the present theoretical picture, and gives us confidence in extrapolating that theory to even higher fields. We point out that the situation was quite the opposite prior to these measurements, with earlier studies[1,3,4] showing a decrease in rate constant with the field increasing up to 10 T, in qualitative disagree-

ment with theory. We now believe that the previous measurements were in fact probing a process other than the pure dipole-dipole mechanism proposed by Kagan et al.[11] It is likely that the previous measurements at moderate field strengths were probing the dipole-exchange recombination process discussed by de Goey et al.[18] By doubling the maximum field and tripling the *range* of field over which data on three-body bulk recombination exists, our new data have dramatically altered our view of how the system behaves. If the new picture which is emerging holds true for surface three-body recombination as well, then Bose-Einstein condensation may be achievable[16] at 27 T in presently available magnet systems.

ACKNOWLEDGMENTS

APPENDIX: EDDY-CURRENT HEATING

We consider a metal in the presence of an oscillating magnetic field: The time-varying magnetic flux through the metal induces a voltage which causes current to flow and leads to dissipation. As an example, consider a cylindrical annulus of outer radius b and inner radius a, and of height h oriented with its symmetry axis parallel to an oscillating magnetic field B. The total heat generated in the metal of resistivity ρ can be obtained by integrating shells of current to obtain an expression for the total power dissipated,

$$P = \frac{h\pi\dot{B}^2}{\mu_0^2 2\rho} \int r^3 dr = \frac{\pi h}{8\rho\mu_0^2}(b^4 - a^4)\dot{B}^2 \propto \frac{\omega^2}{\rho} \ . \quad (A1)$$

This expression is valid in the resistive limit $[\delta \gg (b-a)]$ where δ is the skin depth,

$$\delta = (2\rho/\omega\mu_0)^{1/2} \ , \quad (A2)$$

and ω is the angular frequency, assuming B has a sinusoidal variation. In the inductive limit $(t \gg \delta)$ a sheet of conductor of thickness t and area A has the dissipation

$$P = \frac{B^2}{\mu_0^2}\frac{\rho}{\delta} A \propto \rho^{1/2}\omega^{1/2} \ . \quad (A3)$$

The Bitter magnets in use at the National Magnet Laboratory are characterized by[33]

$$B = B_0 + \sum_n B_n \sin(\omega_n t) \ , \quad (A4)$$

with frequencies and amplitudes given in Table III, so after time averaging we obtain

$$\dot{B}^2 = \tfrac{1}{2}\sum_n \omega_n^2 B_n^2 \ . \quad (A5)$$

TABLE III. Principal ripple frequencies and rms amplitudes measured in a 15-T magnet with $B_0 = 15$ T at the FBNML.

n	$f = \omega/2\pi$ (Hz)	B_n/B_0
1	6	4×10^{-4}
2	24	3×10^{-4}
3	84	6×10^{-4}
4	420	2×10^{-4}

We note that higher frequency components can dominate the heating in the inductive limit. This contribution to the eddy-current heating can easily be suppressed with a copper tubing at $T = 4$ K having a 1-mm wall thickness to shield the ac field.[33]

For (OFHC) copper with $\rho = 7 \times 10^{-3}\ \mu\Omega$ cm at low temperature[34] (impurity limited): $\delta(6\ \text{Hz}) = 1.5$ mm, $\delta(84\ \text{Hz}) = 400\ \mu\text{m}$, and $\delta(720\ \text{Hz}) = 136\ \mu\text{m}$. These skin depths are increased by 10 for aluminum (1100) and by 70 for stainless steel.[34] In a field of 20 T, the magnetoresistance of copper[34] can increase the skin depths listed above by a factor of 4.

For an OFHC sheet of copper of area 1 cm^2 in the inductive limit in a 20-T field as specified above, the heat generated by eddy currents can be of order 1 mW. Whereas for stainless steel the corresponding heat generated is down by a factor of order 10^2.

The formula corresponding to [Eq. (A1)] for a thin sheet of metal of thickness (t) and area (A) with surface oriented parallel to the field is given by,[34]

$$\frac{P}{A} = \left[\frac{B}{\mu_0}\right]^2 \frac{\rho}{\delta}\frac{1}{6}\left[\frac{t}{\delta}\right]^3 \sim \frac{1}{\rho} \ . \quad (A6)$$

These formulas make it apparent why a dramatic reduction in eddy-current heating can be made by the appropriate choice of geometry. For example, consider a solid slab of copper as compared with an equal volume of copper distributed in a laminated structure. For the solid slab, the total heat generated in the resistive limit is proportional to t^3, as indicated in [Eq. (A6)]. For n laminations, however, we must make the substitution,

$$t^3 \rightarrow n\left[\frac{t}{n}\right]^3 \sim \frac{1}{n^2} \ , \quad (A7)$$

so the total heat generated is reduced greatly as the number of laminations (n) increases.

In the case of a thin annulus of radius R and thickness t, a single split down one side breaks up the circular flow of current and reduces the eddy-current heating by roughly $(R/t)^2$, as can be seen by comparing the annulus formula to the thin sheet formula.

For the case of a solid rod (radius R), breaking the rod up into n filaments (radius r) reduces the eddy-current heating by the factor $n(r/R)^4 \sim 1/n$.

To be effective, laminations must be oriented properly. Flat laminations perpendicular to the field have no effect. Cylindrical laminations with their axis parallel to the field also have no effect. Note also that laminations only

help once one is in the resistive limit; in the inductive limit, laminations can make the eddy-current heating worse if the field is allowed to penetrate between the laminations.

Finally, it is interesting to point out that a uniform metal in the resistive limit which obeys the Wiedeman-Franz law will develop temperature gradients which are *independent* of the resistivity, even though the magnitude of eddy-current heating depends inversely on the resistivity:

$$\Delta T \sim P/\kappa \sim 1/\rho\kappa = \frac{1}{LT} \, , \qquad (A8)$$

where the Lorenz number (L) is independent of the material. Essentially, the increased heating which occurs for materials with higher *electrical* conductivity is transported away better by the higher *thermal* conductivity. However, in our experiments, the principal design problem was the reduction of the total heat load which would otherwise overwhelm the dilution refrigerator.

[1]R. Sprik, J. T. M. Walraven, and I. F. Silvera, Phys. Rev. Lett. **51**, 479 (1983); **51**, 942 (1983); R. Sprik, J. T. M. Walraven, and I. F. Silvera, Phys. Rev. B **32**, 5668 (1985).

[2]R. Sprik, Ph.D. thesis, University of Amsterdam, the Netherlands, 1985.

[3]H. Hess, D. A. Bell, G. P. Kochanski. R. W. Cline, D. Kleppner, and T. J. Greytak, Phys. Rev. Lett. **51**, 483 (1983); D. A. Bell, H. F. Hess, G. P. Kochanski, S. Buchman, L. Pollack, Y. M. Xiao, D. Kleppner, and T. J. Greytak, Phys. Rev. B **34**, 7670 (1986); D. A. Bell, Ph.D. thesis, MIT, Cambridge, MA, 1986.

[4]T. Tommila, E. Tjukanov, M. Krusius, and S. Jaakkola, Phys. Rev. B **36**, 6837 (1987); T. Tommila, Ph.D. thesis, University of Turku, Finland, 1987.

[5]A. Einstein, Sitzber. Preuss Akad. Wiss. Physik-Math. I; 3 (1925).

[6]K. Huang, *Statistical Mechanics* (Wiley, New York, 1963).

[7]I. F. Silvera and J. T. M. Walraven, Phys. Rev. Lett. **44**, 164 (1980).

[8]H. F. Hess, G. P. Kochanski, J. M. Doyle, N. Masuhara, D. Kleppner, and T. J. Greytak, Phys. Rev. Lett. **59**, 672 (1987).

[9]N. Masuhara, J. M. Doyle, J. C. Sandberg, D. Kleppner, T. J. Greytak, H. F. Hess, and J. P. Kochanski, Phys. Rev. Lett. **61**, 935 (1988).

[10]R. van Roijen, J. J. Berkhout, S. Jaakkola, and J. T. M. Walraven, Phys. Rev. Lett. **61**, 931 (1988).

[11]Yu. Kagan, I. A. Vartanyants, and G. V. Shlyapnikov, Zh. Eksp. Teor. Fiz. **81**, 1113 (1981). [Sov. Phys.—JETP **54**, 590 (1981)].

[12]L. P. H. de Goey, L. P. J. Driessen, B. J. Verhaar, and J. T. M. Walraven, Phys. Rev. Lett. **53**, 1919 (1984).

[13]L. P. H. de Goey, H. T. C. Stoof, J. M. V. A. Koelman, B. H. Verhaar, and J. T. M. Walraven, Phys. Rev. B **38**, 11221 (1988).

[14]H. T. C. Stoof, L. P. H. de Goey, B. J. Verhaar, and W. Glockle, Jpn. J. Appl. Phys. **26**, Suppl. 26-3, 251 (1986).

[15]H. T. C. Stoof, L. P. H. de Goey, B. J. Verhaar and W. Glöckle, Phys. Rev. **38**, 11221 (1988).

[16]I. F. Silvera, J. D. Gillaspy, and J. G. Brisson, Proceedings of the Conference on Spin Polarized Quantum Systems, Torino, Italy, June 1988 (unpublished).

[17]J. D. Gillaspy, I. F. Silvera, and J. Brook, Phys. Rev. B **38**, 9231 (1988).

[18]L. P. H. de Goey, T. H. M. v. d. Berg, N. Mulders, H. T. C. Stoof, B. J. Verhaar, and W. Glockle, Phys. Rev. B **34**, 6183 (1986).

[19]L. J. Rubin and P. A. Wolff, Phys. Today **37** (8), 24 (1984).

[20]J. G. Brisson and I. F. Silvera, Rev. Sci. Instrum. **57**, 2842 (1986).

[21]A. C. Motta, Rev. Sci. Instrum. **42**, 1541 (1971).

[22]J. T. M. Walraven and I. F. Silvera, Rev. Sci. Instrum. **53**, 1167 (1982).

[23]E. A. Neppiras, Phys. Rep. **61**, 161 (1980).

[24]R. L. Rusby, J. Low Temp. Phys. **58**, 203 (1985).

[25]T. R. Roberts and S. G. Sydoriak, Phys. Rev. **102**, 304 (1956).

[26]G. H. van Yperen, A. P. M. Matthey, J. T. M. Walraven, and I. F. Silvera, Phys. Rev. Lett. **47**, 800 (1981).

[27]This value is from J. R. Eckardt, D. O. Edwards, S. Y. Shen, and F. M. Gasparini, Phys. Rev. B **16**, 1944 (1977); M. Ino, M. Suzuki, and A. J. Ikushima, J. Low Temp. Phys. **61**, 155 (1985), have found a slightly smaller value of 0.3544 ergs cm^{-2}. Our results are fairly insensitive to small changes in the value of γ.

[28]I. F. Silvera and J. T. M. Walraven, *Progress in Low Temperature Physics,* edited by D. F. Brewer (North Holland, Amsterdam, 1986), p. 139.

[29]J. P. Chandler (unpublished).

[30]F. B. Hildebrand, *Introduction to Numerical Analysis* (McGraw-Hill, New York, 1956).

[31]J. D. Gillaspy, I. F. Silvera, and J. S. Brook, *Proceedings of the 18th International Conference on Low Temperature Physics, Kyoto;* Jap. J. Appl. Phys. **26**, Suppl. 26-3, 229 (1987).

[32]P. R. Bevington, *Data Reduction and Error Analysis for the Physical Sciences* (McGraw-Hill, New York, 1969).

[33]E. Meyer, I. Silvera, and B. Brandt (unpublished).

[34]R. P. Reed and A. F. Clark, *Materials at Low Temperatures,* American Society for Metals (Metals Park, Ohio, 1983).

[35]H. P. Godfried, E. R. Eliel, J. G. Brisson, J. D. Gillaspy, C. Mallardeau, J. C. Mester, and I. F. Silvera, Phys. Rev. Lett. **55**, 1311 (1985).

[36]R. M. C. Ahn, J. P. H. W. van den Eijnde, C. J. Reuver, B. J. Verhaar, and I. F. Silvera, Phys. Rev. B **26**, 452 (1982).